SCIENTIFIC REP{O}RTS

OPEN

Hotspot relaxation time of NbN superconducting nanowire single-photon detectors on various substrates

Lu Zhang [1,2,3], Lixing You [1,3], Xiaoyan Yang[1,3], Junjie Wu[1], Chaolin Lv[1,2], Qi Guo[1], Weijun Zhang[1,3], Hao Li[1,3], Wei Peng[1,3], Zhen Wang[1,3] & Xiaoming Xie[1,3]

Hotspot relaxation time (τ_{th}) is one of the essential parameter which defines the maximum count rate of superconducting nanowire single-photon detectors (SNSPDs). We studied the τ_{th} for NbN-based SNSPDs on various substrates using the two-photon detection method based on the pump-probe spectroscopy technique. We observed that τ_{th} strongly increased with increasing bias current in the two-photon detection regime. In addition, the minimum hotspot relaxation time $(\tau_{th})_{min}$ was not significantly affected by the bath temperature; this is different from the previous observations reported for WSi SNSPDs. In addition, a strong dependency of $(\tau_{th})_{min}$ on the substrate was found. The minimum $(\tau_{th})_{min}$ was 11.6 ps for SNSPDs made of 5.5-nm-thick NbN on MgO (100), whereas the maximum $(\tau_{th})_{min}$ was 34.5 ps for SNSPDs made of 7.5-nm-thick NbN on Si (100). We presented a direct correlation between the values of τ_{th} and degrees of disorder of NbN films grown on different substrates.

Superconducting nanowire single-photon detector (SNSPD) is one of the most promising detectors in the near-infrared region owing to its unique combination of high speed, high detection efficiency, small timing jitter, and low dark count rate[1,2]. These features make SNSPD attractive for a variety of applications, especially, quantum information processing[3,4]. In recent years, many experimental and theoretical studies have investigated the detection mechanism to further enhance the count rates[5–7]. The difficulty in achieving high-count-rate SNSPDs stems from their unique internal mechanism of photon detection and the external readout circuit.

A typical SNSPD comprises a meandered nanowire patterned from few-nanometer-thin superconducting films such as NbN or WSi[8,9]. Absorption of a photon in a superconducting nanowire resulted in a non-equilibrium distribution of quasiparticles, with highly energetic hot electrons at a higher temperature than the Cooper pairs. The energy of the excited quasiparticles is redistributed within the electron and phonon system, which lead to an accumulation of quasiparticle excitations just above the energy gap and bring on the formation of a growing hotspot. The phonons in the nanowire dissipate the excess energy into the substrate and relax to the bath temperature; the equilibrium is restored throughout the entire superconducting sample then the hotspot disappears. The process of energy redistributed after the initial absorption of a photon is very fast (~fs) in disordered superconductors. Therefore, the energy transfer and down-conversion process following the absorption of a photon related to the formation and evolution of hotspot (hotspot relaxation process) can be characterized by a single time constant τ_{th} (hotspot relaxation time). The minimum time of SNSPD required for recovery to superconducting state is determined by the hotspot relaxation process. NbN-based SNSPDs have demonstrated intrinsic response times down to a few tens of ps, allowing the count rates to approach the GHz regime[10]. However, being limited by their large kinetic inductance (L_k) and the input impedance of the readout circuit (R_s), the devices have reset times that are several orders of magnitudes larger (~ns and larger) than their intrinsic response time. Reducing L_k and/or increasing R_s lead to a high count rate; however, the improvement in count rate is further restricted by the negative electro-thermal feedback[11]. In addition, for superconducting materials with slow hotspot relaxation

[1]State Key Laboratory of Functional Material for Informatics, Shanghai Institute of Microsystem and Information Technology, Chinese Academy of Sciences, Shanghai, 200050, China. [2]University of Chinese Academy of Sciences, Beijing, 100049, China. [3]Center for Excellence in Superconducting Electronics, Chinese Academy of Sciences, Shanghai, 200050, China. Correspondence and requests for materials should be addressed to L.Y. (email: lxyou@mail.sim.ac.cn)

1

Sample	Substrate material	d (nm)	w (nm)	s (nm)	I_{sw} (μA)	J_{sw} (MA/cm²)	$(\tau_{th})_{min}$ (ps)
#1	MgO (100)	5.5	90	110	33	6.7	11.6 ± 0.1
#2	MgO (100)	5.5	105	110	40	6.9	12.2 ± 0.1
#3	MgO (100)	5.5	120	110	51.5	7.8	12.6 ± 0.1
#4	MgF₂ (110)	4.5	90	110	22	5.4	19.7 ± 0.1
#5	Al₂O₃ (0001)	7	130	70	21.5	2.4	22.5 ± 0.7
#6	SiO₂/Si (100)	7	90	110	21	3.3	22.7 ± 0.1
#7	Si (100)	7.5	90	110	19	2.8	34.5 ± 0.3

Table 1. Substrate material, film thickness (d), nanowire linewidth (w), space (s), switching current (I_{sw}), switching current density (J_{sw}), and minimum hotspot relaxation time (τ_{th})$_{min}$ for the seven SNSPDs.

process, devices would latch into a finite voltage state instead of self-resetting to the superconducting state after detecting a photon[12]. Therefore, τ_{th} is an important parameter that defines the maximum achievable count rate.

To quantitatively study hotspot relaxation process, several experiments have been conducted. In 2012, Heeres *et al*. proposed a quantum pump-probe technique based on the use of correlated photons from spontaneous parametric down-conversion (SPDC); they derived that the τ_{th} of an approximately 4-nm-thick NbN film grown on a sapphire substrate is ~15 ps and independent of the SPDC pump power and bias current[13]. In 2013, Zhou *et al*. demonstrated a novel method to measure ultrasensitive N-photon interferometric autocorrelation and determined that the τ_{th} of an approximately 4.3-nm-thick NbN film prepared on GaAs substrates is ~20 ps[14]. In 2016, Marsili *et al*. proposed a new technique that combined the pump-probe detection technology and Mach-Zehnder interferometer. They found that the τ_{th} of ~5-nm-thick WSi film on SiO₂/Si substrates varied from ~80 ps to ~800 ps with increasing bias current (I_b), bath temperature (T_B), or photon energy[15].

To identify the key factors affecting the relaxation time of NbN SNSPDs, we systematically studied the τ_{th} of NbN SNSPDs via two-photon detection experiments based on the pump-probe spectroscopy technique. Devices with various geometric parameters (e.g., film thickness and nanowire linewidth) were fabricated on different substrates: MgO (100), MgF₂ (110), Al₂O₃ (0001), Si (100), and SiO₂/Si (100). The τ_{th} values of different SNSPDs were measured and compared. Besides, the temperature dependence (2.15–5 K) of τ_{th} was also analyzed.

Results

Determination of τ_{th}. SNSPD devices with different nanowire linewidth/space ratio (w/s) were fabricated from NbN films deposited on different substrates and cooled down for the characterization (see Table 1). Detailed information concerning device preparation, characterization and measurement setup can be found in the methods' section below. The single-photon regime in SNSPD can be achieved when I_b is biased close to the switching current (I_{sw}). When lowering I_b, the energy of a single photon is insufficient to create a response pulse and the detector only responds to two or more photons[10,14,15]. Herein, we introduced the two-photon detection method, wherein the response pulse is triggered when the two incident photons separated by the time delay (t_D) generate two hotspots that overlap spatially and temporally. According to recent research, the probability of having two absorbed photons of incident photons can be given by $(\eta\mu)^2/2$, where η is the two-photon detection efficiency and μ is the average number of photons per pulse[15,16]. When t_D was longer than τ_{th}, the response probability is approximately equal to the sum of each pulse of $(\eta\mu)^2$. When t_D was shorter than τ_{th}, the increased mean photon number doubled the response probability to $2(\eta\mu)^2$. Consequently, the evolution of hotspot relaxation process differed from that of SNSPD recovery.

First, Sample #6 was tested (7-nm-thick NbN/SiO₂/Si (100) and 90-nm-wide nanowire with a 110-nm space) at T_B of 2.15 K. The I_{sw} of the device was approximately 21 μA. To distinguish the bias current range for two-photon detection, the count rates were measured as a function of the light power (average photon number per pulse) at several I_b values of 12.5 μA, 12 μA, 11 μA, 10 μA, and 7 μA. As shown in Fig. 1(a), the solid lines are fits to the measured data in the log-log scale. At I_b = 12.5 μA, and 7 μA, the fitted slope of 1.02 ± 0.01, and 3.05 ± 0.02 indicating that the detector operates in the single, and three-photon detection regime. At I_b of 12 μA, 11 μA, and 10 μA, the slopes of the fitting lines are 1.91 ± 0.02, 1.99 ± 0.01, and 2.04 ± 0.01, respectively. Therefore, the detector is dominated by two-photon detection for bias current 10 μA ≤ I_b ≤ 12 μA. We note that, there is no sharp boundary between either single or two-photon detection regime (~12 μA), and two-photon and three-photon regime (~10 μA). However, with the current lower than 10 μA, the count rate is too low to study with the fixed average photon number. With the current higher than 12.0 μA, the single-photon detection will be dominant so we cannot obtain the accurate τ_{th} based on Lorentz function fitting (see Fig. 1(b)). Therefore, the bias range of 10–12 μA is suitable for studying the τ_{th}. Figure 1(b) illustrates the photon-response count rate (PCR) as a function of t_D at different I_b values from 10 μA to 12.5 μA. The measured data were fitted with a Lorentz function and normalized to 2 at t_D = 0 ps, ignoring the optical interference in the range −2 ps ≤ t_D ≤ 2 ps. At I_b = 12.5 μA, the PCR was irrelevant to t_D as the detector was nearly working in the one-photon detection regime. When I_b was lowered to 10 μA, the normalized PCR declined from 2 to ~1, with t_D increasing from 0 ps to ~150 ps[15,17]. In particular, the half width of this peak directly corresponds to τ_{th}. Figure 1(c) shows τ_{th} as a function of I_b extracted from the data in Fig. 1(b). The minimum value of the hotspot relaxation time $(\tau_{th})_{min}$ was 22.7 ps ± 0.1 ps at I_b = 10 μA. Additionally, τ_{th} increased to 79.5 ps ± 1.5 ps, whereas I_b increased to 12 μA. These trends have also been reported for WSi SNSPDs and NbN waveguide-integrated SNSPDs, for which self-recombination rather than diffusive expansion explained the strong dependence of τ_{th} on I_b[18].
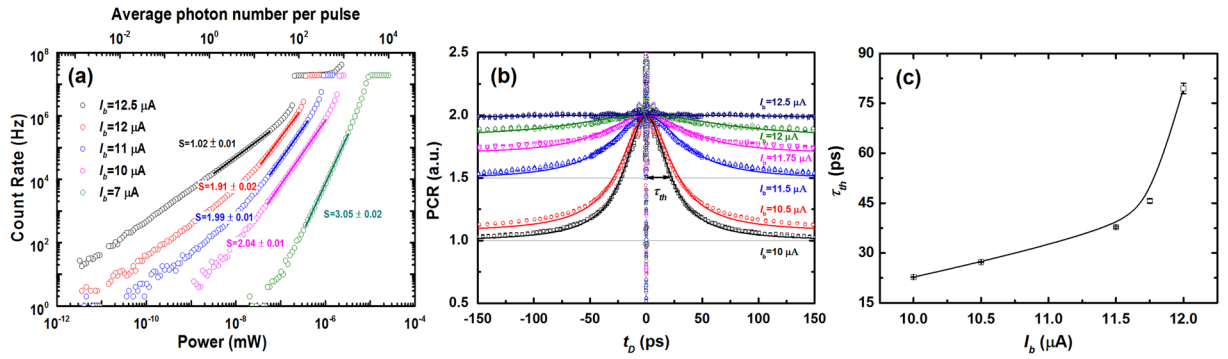
Figure 1. (**a**) Count rates as a function of light power (average photon number per pulse) at five different I_b values. The measured points, denoted by the open circles, were fitted with straight lines in the log–log scale. The slopes of the fitting lines are 1.02 ± 0.01, 1.91 ± 0.02, 1.99 ± 0.01, 2.04 ± 0.01, and 3.05 ± 0.02, respectively. (**b**) Normalized PCR as a function of t_D, which is measured when the detector operated in the two-photon detection regime at I_b values of 10, 10.5, 11.5, 11.75, and 12 μA; I_b of 12.5 μA corresponding to the one-photon detection regime is also shown for comparison. The measured data were fitted with a Lorentz function. The black arrow denotes the half width at half maximum of the curve, which directly corresponds to τ_{th} measured at $I_b = 10$ μA. (**c**) τ_{th} as a function of I_b extracted from the data in (**b**).
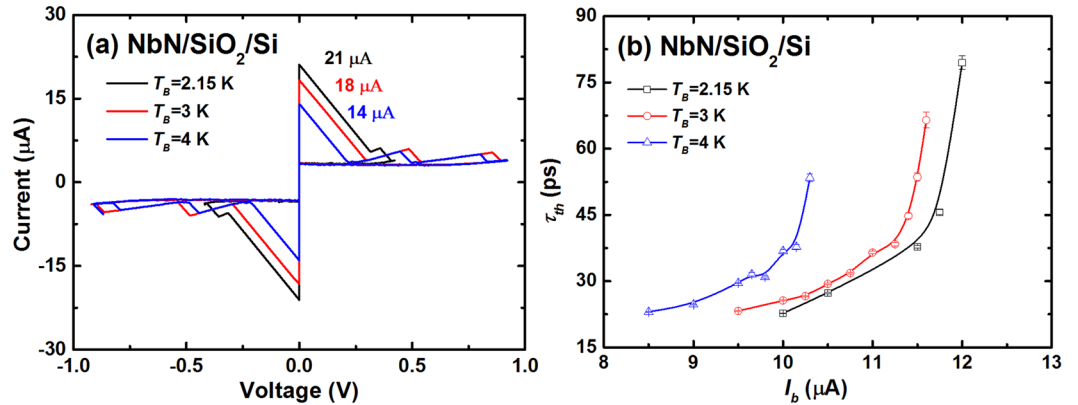

Figure 2. (**a**) I-V curves and (**b**) τ_{th} as a function of I_b measured at T_B values of 2.15 K, 3 K, and 4 K, respectively, for Sample #6.

Dependence of τ_{th} on bath temperature. To investigate the temperature dependence of τ_{th}, we tuned the T_B of SNSPDs from 2.15 K to 4 K using the resistive heater. Figure 2(a) shows the current-voltage (I-V) characteristics of Sample #6 at three different temperatures (2.15 K, 3 K, and 4 K). I_{sw} decreased from 21 μA to 14 μA with increasing T_B. As a result, the two-photon detection ranges changed to $10\,\mu A \leq I_b \leq 12\,\mu A$ (2.15 K), $9.5\,\mu A \leq I_b \leq 11.6\,\mu A$ (3 K), and $8.5\,\mu A \leq I_b \leq 10.3\,\mu A$ (4 K). Then, the I_b dependence of τ_{th} at different T_B values were studied; τ_{th} gradually increased with I_b and presented a considerable change around the one-photon detection regime for all T_B values (Fig. 2(b)). However, the τ_{th}-I_b curve shifted to a smaller I_b with increasing T_B owing to the change of the two-photon detection range. In addition, at a fixed I_b, τ_{th} increased with T_B; this could be attributed to the decreased electron relaxation rate at high T_B. However, the $(\tau_{th})_{min}$ values at T_B values of 2.15 K, 3 K, and 4 K were measured to be 22.7 ps ± 0.1 ps, 23.2 ps ± 0.1 ps, and 23.0 ps ± 0.1 ps, respectively. The results agree well with each other, and we saw a saturated trend of τ_{th} with decreasing the current, suggesting that the minimum hotspot relaxation time might be independent of T_B. However, it is difficult to verify it by further decreasing the current since the device no longer worked in the two-photon detection regime anymore. This is different from the results reported for WSi SNSPDs, where $(\tau_{th})_{min}$ increased with T_B from 250 mK to 2 K[15]. Possibly, the smaller I_{sw} of WSi SNSPDs at higher temperatures restricts the ability to reach the lowest bias in the two-photon detection regime owing to the limit of the readout circuit. In other words, the $(\tau_{th})_{min}$ of WSi SNSPDs might be smaller at high temperatures as well.

Dependence of τ_{th} on nanowire linewidth. It has been well established that the w of nanowire affects not only the optical absorption but also the intrinsic detection efficiency of SNSPD[8,19]. To understand the influence of w on τ_{th}, three different SNSPDs were fabricated on MgO substrate, wherein w was designed to be 90, 105, and 120 nm, respectively. The s value was set to 110 nm. The measured w/s is consistent with the design as the EBL and RIE processes were optimized. The other parameters are listed as Samples #1–3 in Table 1.
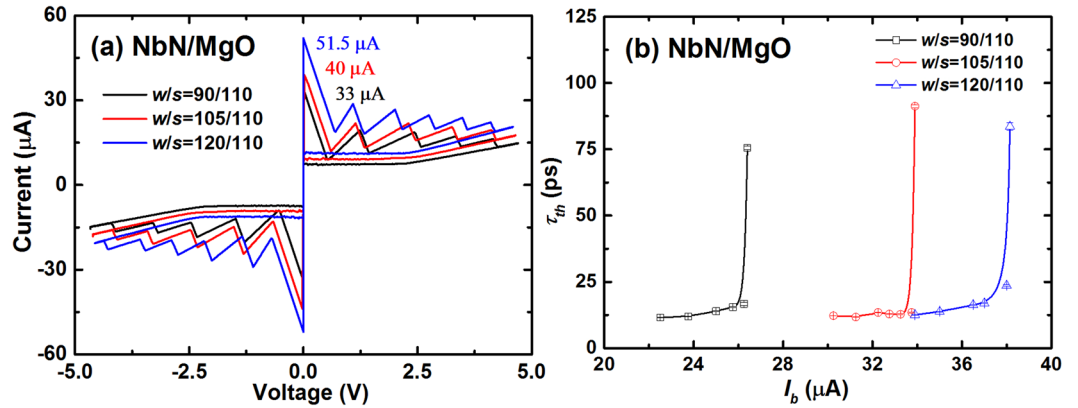
Figure 3. (**a**) *I-V* curves and (**b**) τ_{th} as a function of I_b at T_B values of 2.15 K for Sample #1–3 with different *w/s*.
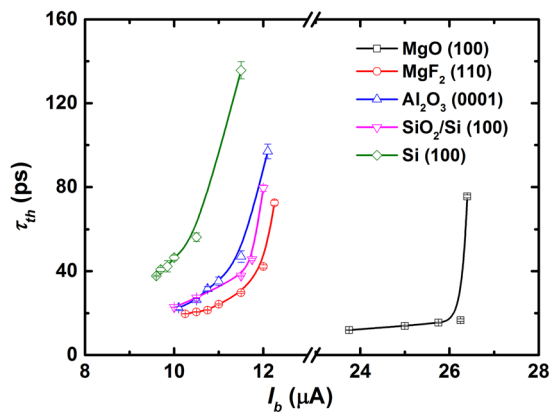

Figure 4. τ_{th} as a function of I_b at T_B values of 2.15 K for various substrates.

Figure 3(a) shows the *I-V* curves of the SNSPDs with three different *w* values (90, 105, and 120 nm) that give I_{sw} values of 30, 40, and 51.5 μA respectively. Similarly, we obtained the relation of τ_{th} as a function of I_b for the three SNSPDs, as shown in Fig. 3(b). The trend displayed in the figure is comparable to that of Sample #6, and the curve shifts to the right with increasing *w* while maintaining the shape similarity. The $(\tau_{th})_{\min}$ values for the three SNSPDs were determined to be 11.6 ps ± 0.1 ps, 12.2 ps ± 0.1 ps, and 12.6 ± 0.1 ps, respectively. The deviations were lesser than 1 ps. The slight increase in $(\tau_{th})_{\min}$ with increasing *w* is explained by the presence of less thermal relaxation channels in the center of the nanowire as opposed to at the sides of the nanowire. In addition, the values are only half of those obtained for Sample #6; this is further discussed in the next section.

Dependence of τ_{th} on the substrate. A variety of substrates, such as Si, MgO, MgF$_2$, and Al$_2$O$_3$, have been used to grow ultrathin NbN films for fabricating SNSPDs[20–22]. To investigate the effect of substrates on τ_{th}, we measured and compared the τ_{th} of NbN SPSPDs on different substrates [Si (100), MgO (100), MgF$_2$ (110), Al$_2$O$_3$ (0001), and SiO$_2$/Si (100)].

Figure 4 shows τ_{th} as a function of I_b at $T_B = 2.15$ K for SNSPDs on various substrates. All SNSPDs showed a similar increase in τ_{th} with increasing I_b. The $(\tau_{th})_{\min}$ values are summarized in Table 1 and follow the simple relation $(\tau_{th})_{\min}(\text{MgO}) \leq (\tau_{th})_{\min}(\text{MgF}_2) \leq (\tau_{th})_{\min}(\text{Al}_2\text{O}_3) \leq (\tau_{th})_{\min}(\text{SiO}_2/\text{Si}) \leq (\tau_{th})_{\min}(\text{Si})$. The maximum difference of $(\tau_{th})_{\min}$ is roughly three times. The smallest $(\tau_{th})_{\min}$ (11.6 ps ± 0.1 ps) was obtained from the MgO (100) substrate, and the largest $(\tau_{th})_{\min}$ (34.5 ps ± 0.3 ps) was obtained from the Si (100) substrate. Typically, τ_{th} is controlled by carrier diffusion as well as by the recombination time of the quasiparticles, which is indeed related to the degrees of disorder of the materials[15,23]. In other words, a film with a lower disorder would have a smaller $(\tau_{th})_{\min}$.

Role of disorder on τ_{th}. The superconducting properties of NbN films are determined by many parameters of the films. One of the key parameters is actually the film crystal structure, which is strongly influenced by not only the substrate material but many other parameters including the deposition condition. Meanwhile, NbN is a conventional s-wave superconductor and the superconducting properties of the NbN ultrathin film can be partially characterized by its degrees of disorder, which is related to not only the substrate material, but also the film thickness. The degrees of disorder of NbN films on two substrates MgO and SiO$_2$/Si were quantitatively analyzed. First, we measured the normalized resistance (R_N) as a function of T_B for the 5.5-nm-thick NbN/MgO and 7-nm-thick NbN/SiO$_2$/Si substrates under different magnetic fields via transport measurements using a physical
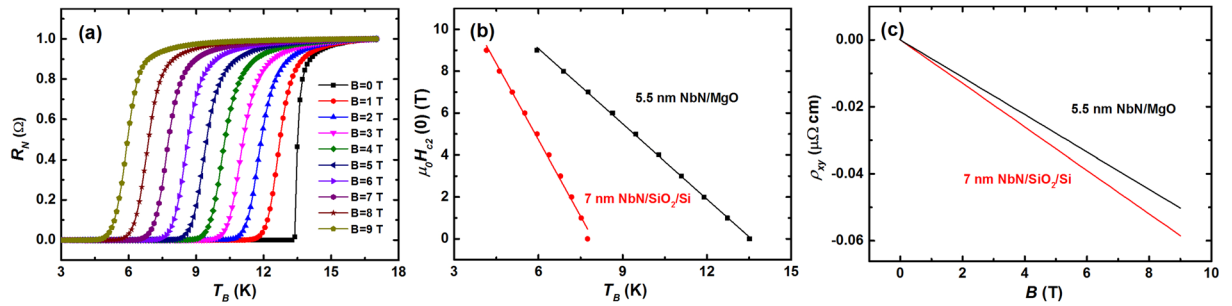
Figure 5. (a) R_N as a function of T_B for 5.5-nm-thick NbN on MgO (100) under different magnetic fields. (b) $\mu_0 H_{c2}$ as a function of T_B for 5.5-nm-thick NbN on MgO (100) and 7-nm-thick NbN on SiO$_2$/Si (100). The solid lines are linear fits to the data. (c) ρ_{xy} as a function of B at 25 K for the two samples.

Substrate material	d (nm)	T_c (K)	ρ_n (μΩ cm)	$\mu_0 H_{c2}$ (0) (T)	ξ_{GL} (nm)	D (cm²/s)	l (Å)	$k_F l$
MgO (100)	5.5	13.51	154	11.17	5.43	0.92	3.56	5.31
SiO$_2$/Si (100)	7	7.71	562	12.56	5.12	0.47	1.08	1.53

Table 2. Critical temperature (T_c), normal resistivity (ρ_n), upper critical field [$H_{c2}(0)$], Ginzburg–Landau coherence length (ξ_{GL}), electron diffusion coefficient (D), mean electronic free path (l), and Ioffe–Regel parameter ($k_F l$) for the 5.5-nm-thick NbN/MgO (100) and 7-nm-thick NbN/SiO$_2$/Si (100) samples.

property measurement system. To accurately determine the resistivity (ρ_n), the electrical resistance (R) was measured on a $4\,\mu m \times 40\,\mu m$ microbridge using the standard four-probe method. Figure 5(a) shows the R_N-T_B relations for the 5.5-nm-thick NbN/MgO sample. The upper critical field (H_{c2}) values at different temperatures were then determined at the point where R_N becomes 50% of its normal value. The $\mu_0 H_{c2}$-T_B relations for the two samples are shown in Fig. 5(b). In the dirty limit of a superconductor film e.g., NbN, the mean electronic free path (l) is shorter than the Ginzburg–Landau coherence length (ξ_{GL}). Then, $H_{c2}(0)$, ξ_{GL}, and the electron diffusion coefficient (D) are obtained from $H_{c2}(0) = 0.69 T_c (dH_{c2}/dT)|_{T=T_c}$, $\xi_{GL} = \sqrt{\Phi_0 / 2\pi H_{c2}(0)}$, and $D = -4 k_B / (\pi e d H_{c2}/dT)$, respectively, where Φ_0 is the flux quantum, k_B is the Boltzmann constant, and e is the electron charge[24,25]. For NbN films epitaxially grown on the MgO substrate, the obtained D value was 0.92 cm²/s, which is approximately twice the value of the film on the SiO$_2$/Si substrate (0.47 cm²/s). The larger value of D suggests the presence of fewer defects and vacancies in the samples. The calculated ξ_{GL} values were 5.43 nm and 5.12 nm for the 5.5-nm-thick NbN/MgO and 7-nm-thick NbN/SiO$_2$/Si samples, respectively.

Next, Hall measurement was performed using a four-probe AC technique. Figure 5(c) shows the Hall resistivity (ρ_{xy}) as a function of B for the two samples measured at 25 K. The electron density (n) and the Ioffe–Regel parameter ($k_F l$) are calculated from $n = 1/R_H e$, $k_F = (3\pi^2 n)^{1/3}$, and $l = \rho_n n e^2 / \hbar k_F$, respectively, where $R_H = \rho_{xy}/H$ is determined from the slope shown in Fig. 5(c). All the obtained values are listed in Table 2. As expected, $l < \xi_{GL}$, indicating that all NbN films are in the dirty limit irrespective of which substrate is used. However, the $k_F l$ values described herein range from moderately disordered (5.31) to strongly disordered (1.53), suggesting that NbN grown on the MgO (100) substrates exhibits a less disordered structure. The film superconductivity decreases with increasing disorder. The J_{sw} values listed in Table 1 are also confirmed the above judgments to some extent.

Discussion

The minimum $(\tau_{th})_{min}$ measured in our NbN SNSPDs is about only one in seven of WSi SNSPDs', indicating a significant difference in material properties. The direct method to decrease τ_{th} is to decrease the degrees of disorder of the materials. However, how to decrease τ_{th} together with optimizing other parameters such as intrinsic detection efficiency still remains an open question, which is very interesting for not only understanding the mechanism of SNSPD but also the practical SNSPD with high performance.

In summary, the τ_{th} of NbN SNSPDs on various substrates were investigated with a two-photon detection measurement technique. The experimental setup was based on pump-probe spectroscopy, wherein the laser pulses were separated by time delays tuned in a wide range. To realize two-photon detection in a reasonable bias range, the typically average photon number per pulse is set as 40. The high average photon number per pulse guarantee the data collection in a reasonable time (one dot per hour) compared with the correlated photon-pair source based on SPDC.

Our results show that the bath temperature and nanowire linewidth do not significantly affects $(\tau_{th})_{min}$, i.e. they contribute less to the intrinsic upper limit of the count rate of SNSPD. However, $(\tau_{th})_{min}$ is strongly affected by the substrate because the degrees of disorder of NbN films are different. Epitaxially grown 5.5-nm-thick NbN on MgO (100) has a minimum $(\tau_{th})_{min}$ of 11.6 ps, and amorphous 7.5-nm-thick NbN on Si (100) has a maximum $(\tau_{th})_{min}$ of 34.5 ps. As a result, it is important to choose a suitable substrate if one wants to find lower τ_{th}. Besides, one may further study NbN films deposited on different substrates with different deposition conditions
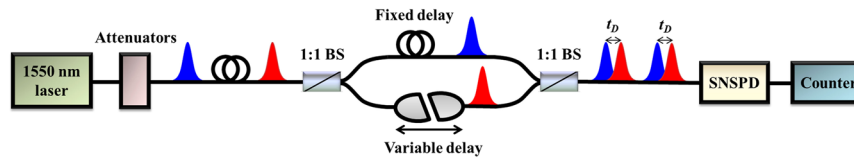
Figure 6. Schematic of the experimental setup for the τ_{th} measurements. Two fiber beam splitters (BS) and a motorized delay line were used to control the t_D between the two pulses.

to further identify the minimum of τ_{th}. It may guide the further studies in the community on not only the physics of ultrathin superconducting films, but also the practical SNSPD with high count rate. Beyond that, the results are also interesting for the study of other superconducting sensors/detectors based on hot-electron effect, for example, hot-electron mixers.

Methods

Device fabrication.   Ultrathin NbN films were synthesized through reactive DC magnetron sputtering of an 8-inch Nb target in an $Ar + N_2$ gas mixture at room temperature. The typical background pressure was 9×10^{-6} Pa. The flow rates of Ar and N_2 were set to 30 sccm and 4 sccm, respectively, under a total pressure of 0.27 Pa. The DC magnetron power was provided by current-regulated power supply set at 2.2 A with a resulting voltage of 270 V. The deposition rate was 6 Å/s, calibrated by X-ray reflectivity. The substrates used for film growth were Si (100) with its native oxide, MgO (100), MgF_2 (110), Al_2O_3 (0001), and Si (100) with a 253-nm-thick buffering SiO_2 layer. Prior to film deposition, all the substrates were cleaned by Argon ion-beam etching in a cleaning chamber. It is worth noting that the etching process removed native oxides of the Si (100) substrate. Because the MgO (100) and MgF_2 (110) substrates allow the epitaxial growth of NbN films, NbN films on these substrates have higher critical temperature T_c than those on the Al_2O_3 (0001), SiO_2/Si (100), and Si (100) substrates. To optimize the device performance, films with different thickness (d) values, i.e., 5.5, 4.5, 7, 7, and 7.5 nm were synthesized on the MgO (100), MgF_2 (110), Al_2O_3 (0001), SiO_2/Si (100), and Si (100) substrates, respectively. The films were structured into a conventional meandered nanowire structure, which covered a 15 μm-diameter area. All nanowire structures were patterned by electron-beam-lithography (EBL) with PMMA950-A2 as the e-beam resist. Electrode structures were formed by reactive ion etching (RIE) in the CF_4 gas. Seven SNSPDs with different nanowire linewidth/space ratio (w/s) were fabricated. The detailed parameters of these SNSPDs are listed in Table 1.

Measurement setup.   The experimental setup for τ_{th} measurement is shown in Fig. 6. The source of optical excitation is a 20-MHz mode-locked fiber laser with a 1550-nm wavelength, 500-fs pulse duration, and a typical maximum average output power of 2 mW. Laser pulses are attenuated and then divided by a 1:1 fiber beam splitter. One part of the pulse is sent to a fixed fiber, whereas the other part is sent to a motorized delay line. The time delay t_D between the two pulses can be controlled by tuning the motorized delay line with a precision of ±0.01 ps. The two pulses are combined again on a 1:1 fiber beam splitter and then coupled to the SNSPDs. The measurements for the SNSPDs are performed in a Gifford–McMahon cryocooler at 2.15–5 K. A resistive heater is placed near the sample to tune the temperature of SNSPDs.

References

 1. Dauler, E. A. *et al.* Review of superconducting nanowire single-photon detector system design options and demonstrated performance. *Opt. Eng.* **53**, 081907 (2014).
 2. Natarajan, C. M., Tanner, M. G. & Hadfield, R. H. Superconducting nanowire single-photon detectors: physics and applications. *Supercond. Sci. Technol.* **25**, 063001 (2012).
 3. Wang, Z., Miki, S. & Fujiwara, M. Superconducting Nanowire Single-Photon Detectors for Quantum Information and Communications. *Ieee. J. Sel. Top. Quant* **15**, 1741–1747 (2010).
 4. Hadfield, R. H. Single-photon detectors for optical quantum information applications. *Nat. Photonics* **3**, 696–705 (2007).
 5. Renema, J. J. *et al.* Experimental test of theories of the detection mechanism in a nanowire superconducting single photon detector. *Phys. Rev. Lett.* **112**, 117604 (2014).
 6. Annunziata, A. J. *et al.* Reset dynamics and latching in niobium superconducting nanowire single-photon detectors. *J. Appl. Phys.* **108**, 084507 (2010).
 7. Engel, A., Renema, J. J., Il'in, K. & Semenov, A. Detection mechanism of superconducting nanowire single-photon detectors. *Supercond. Sci. Technol.* **28**, 114003 (2015).
 8. Li, H. *et al.* Large-sensitive-area superconducting nanowire single-photon detector at 850 nm with high detection efficiency. *Opt. Express* **23**, 17301–17308 (2015).
 9. Marsili, F. *et al.* Detecting single infrared photons with 93% system efficiency. *Nat. Photonics* **7**, 210–214 (2013).
10. Gol'tsman, G. N. *et al.* Picosecond superconducting single-photon optical detector. *Appl. Phys. Lett.* **79**, 705 (2001).
11. Kerman, A. J., Yang, J. K. W., Molnar, R. J., Dauler, E. A. & Berggren, K. K. Electrothermal feedback in superconducting nanowire single-photon detectors. *Phys. Rev. B* **79**, 100509 (2009).
12. Shibata, H., Takesue, H., Honjo, T., Akazaki, T. & Tokura, Y. Single-photon detection using magnesium diboride superconducting nanowires. *Appl. Phys. Lett.* **97**, 212504 (2010).
13. Heeres, R. W. & Zwiller, V. Superconducting detector dynamics studied by quantum pump-probe spectroscopy. *Appl. Phys. Lett.* **101**, 112603 (2012).
14. Zhou, Z. *et al.* Ultrasensitive N-photon interferometric autocorrelator. *Phys. Rev. Lett.* **110**, 133605 (2013).
15. Marsili, F. *et al.* Hotspot relaxation dynamics in a current-carrying superconductor. *Phys. Rev. B* **93**, 094518 (2016).
16. Bitauld, D. *et al.* Nanoscale optical detector with single-photon and multiphoton sensitivity. *Nano. Lett.* **10**, 2977–2981 (2010).
17. Ferrari, S. *et al.* Hot-spot relaxation time current dependence in niobium nitride waveguide-integrated superconducting nanowire single-photon detectors. *Opt. Express* **25**, 8739 (2017).

18. Kozorezov, A. G. *et al.* Quasiparticle recombination in hotspots in superconducting current-carrying nanowires. *Phys. Rev. B* **92**, 064504 (2015).
19. Guo, Q. *et al.* Single photon detector with high polarization sensitivity. *Sci. Rep.* **5**, 9616 (2015).
20. Yang, X. *et al.* Superconducting nanowire single photon detector with on-chip bandpass filter. *Opt. Express* **22**, 16267–16272 (2014).
21. Wu, J. J. *et al.* NbN superconducting nanowire single-photon detector fabricated on MgF$_2$ substrate. *Supercon. Sci. Technol.* **29**, 065011 (2016).
22. Henrich, D. *et al.* Broadening of hot-spot response spectrum of superconducting NbN nanowire single-photon detector with reduced nitrogen content. *J. Appl. Phys.* **112**, 074511 (2012).
23. Leo, A. *et al.* Quasiparticle scattering time in niobium superconducting films. *Phys. Rev. B* **84**, 014536 (2011).
24. Chockalingam, S. P., Chand, M., Jesudasan, J., Tripathi, V. & Raychaudhuri, P. Superconducting properties and Hall effect of epitaxial NbN thin films. *Phys. Rev. B* **77**, 214503 (2008).
25. Lin, S. Z. *et al.* Characterization of thin-film NbN superconductor for single-photon detection by transport measurements. *Phys. Rev. B* **87**, 2450–2458 (2013).

Acknowledgements

Author Contributions

L.Z. and L.X.Y. designed the experiment, analyzed the data and wrote the paper. L.Z. and X.Y.Y. performed the measurements. L.Z. performed the thin film deposition and J.J.W. and W.J.Z. fabricated the SNSPD devices. C.L.L., Q.G. and H.L. provided assistance in the experiment. W.P., Z.W. and X.M.X. discussed the results. All authors reviewed the manuscript.

Additional Information